Original Research

Advances in Structural Engineering

Flexural capacity enhancing of notched steel beams by combining shape memory alloy wires and carbon fiber-reinforced polymer sheets

Advances in Structural Engineering
2023, Vol. 0(0) 1–13

DOI: 10.1177/13694332231168416
journals.sagepub.com/home/ase
SAGE

Jun Deng[1], Zhongyu Fei[1], Junhui Li[1,2] and Haifan Huang[3]

Abstract

Combining shape memory alloy (SMA) and carbon fiber-reinforced polymer (CFRP) sheet can achieve a self-stressing SMA-CFRP composite, providing an innovative prestressing method for steel elements. This study applied SMA(Ni–Ti–Nb) wires and CFRP sheets to achieve composite strengthening for notched steel beams. The effectiveness of SMA-CFRP composite for flexural strengthening of notched steel beams was evaluated, and the formula for the maximum allowable moment of the strengthened beams with SMA-CFRP composites was proposed. The four-point bending test results showed that the ultimate load and flexural stiffness of the strengthened beams with SMA-CFRP composites increased by 79.2% and 57.9% more than those of the unstrengthened beams. By comparison, the CFRP-only and SMA-only strengthened beams merely achieved half the ultimate load and flexural stiffness over the strengthened beams with SMA-CFRP composite. Besides, compared to the unstrengthened beams, the notch tip yield load for the strengthened beam with SMA-CFRP composite was increased by 230%, while the notch tip yield load for strengthened beams with CFRP-only and SMA-only just increased by 70% and 125%. These indicate that the SMA-CFRP composite strengthening can significantly delay crack propagation and improve the load capacity and stiffness of notched steel beams. Moreover, the analytical results of the maximum allowable moment were in good agreement with experimental results, indicating the accuracy of the proposed analytical equations.

Keywords

notched steel beam, carbon fiber-reinforced polymer, shape memory alloy, flexural strengthening, bearing capacity

Introduction

Carbon fibre reinforced polymer (CFRP) has been widely used for strengthening steel structures due to its high strength, light weight, and high durability (Deng et al., 2004; Deng and Lee, 2007; Zhao and Zhang, 2007). After CFRP external bonding, the load capacity, stiffness, and fatigue resistance can be significantly improved for steel members (Hollaway, 2010; Yu and Wu, 2017). However, premature debonding, the most common failure mode for CFRP-strengthened steel members, leads to low strength utilization of CFRP and minimal crack impedance. To overcome this problem, a prestressed CFRP strengthening method was developed (Ghafoori et al., 2012). Prestressed CFRP can apply compressive stress to strengthened steel members and cause a crack closure effect, significantly enhancing static and fatigue performance(Deng et al., 2022; Hu et al., 2022; Li et al., 2018, 2022). Besides, the prestressed CFRP also can be used to reinforce steel columns against overall buckling (Hu and Feng, 2021). In addition, the end anchorage system is crucial to the prestressing technique for resisting high interfacial stress and preventing premature debonding (Ghafoori et al., 2018; Hosseini et al., 2019; Li et al., 2018). As reported (Kianmofrad et al., 2017), the CFRP plate is usually pretensioned to the designed prestressing level by an independent reaction frame, and then the CFPR plates are locked using a mechanical clamp. This prestressing technique is mainly suitable for laboratory applications but less

[1]School of Civil Engineering, Guangzhou University, Guangzhou, China
[2]School of Transportation, Civil Engineering and Architecture, Foshan University, Foshan, China
[3]School of Civil and Transportation Engineering, Guangdong University of Technology, Guangzhou, China

Corresponding author:
Junhui Li, School of Transportation, Civil Engineering and Architecture, Foshan University, Foshan 528225, China.
Email: jhli@fosu.edu.cn

useful for on-site prestressing of the CFRP plates due to the requirement of hydraulic jacks and complex prestressing setup. Hence, a new prestressing strengthening technique should be studied for metallic structures.

Predeformed shape memory alloy (SMA) shows the unique capability to recover its original shape by a subsequent heating and cooling process (Bollas et al., 2007; Cladera et al., 2014; Mohd Jani et al., 2014). Based on this capability, if the predeformed SMA is attached to the structural element and then heated, the compressive force (prestressing force) can be produced due to the contraction of the SMA (Hosseini et al., 2018). Predeformed SMA has been successfully employed in strengthening concrete (Gholampour and Ozbakkaloglu, 2018; Li et al., 2008; Parvin and Raad, 2018; Shahverdi et al., 2016) and steel structures (Deng et al., 2023; Izadi et al., 2018a; Zareie et al., 2020). Izadi et al. (Izadi et al., 2018a; 2019) developed an SMA system for steel member strengthening and found that approximately 430 MPa of prestressing can be produced after thermal activation of SMA strips. Heat-activated SMA strips can apply considerable compressive stress to cracked steel plates, resulting in a significant increase in fatigue performance (Izadi et al., 2018a). The mechanical anchor is important for SMA strengthening to connect SMA strips to steel structures, and friction clamps (Izadi et al., 2018b) and nail anchor systems (Fritsch et al., 2019) were developed. However, these mechanical anchors need holes machined into the steel substrate to install the mechanical anchorage system, leading to potential problems of local stress concentrations and a decrease in the cross-sectional area.

In addition, an SMA-CFRP composite was developed by sandwiching prestrained SMA wires between CFRP materials (Abdy et al., 2018; Li et al., 2020), which offers both the benefits of the prestress of SMA and the high elastic modulus of CFRP. Li et al. (Li et al. (2020)) studied the fatigue behaviour of central cracked steel plates reinforced by SMA-CFRP composites. The results showed that the fatigue lives were extended to 2.7 times that of the specimen with normal modulus CFRP. However, this preparation method of the SMA-CFRP patch has a limitation because epoxy resin adhesive, which is sensitive to temperature (Galvez et al., 2019; He et al., 2020; Ke et al., 2020), was used for SMA wire embedment. The glass transition temperature of the adhesive is generally in the range of 45–82°C (He et al., 2020), limiting the maximum heating temperature of the SMA. Thus, the SMA-CFRP patch cannot generate sufficient recovering force. To solve this problem, EI-Tahan et al. (El-Tahan et al., 2015; El-Tahan and Dawood, 2018) presented a new approach in which the prestressing force is applied by the shape memory effect of NiTiNb SMA wires. The prestrained SMA wires were first embedded into two FRP tabs. Then, the cured tabs were bonded to a cracked steel element using a structural adhesive to anchor the SMA wires to the structure on either side of the crack. After that, the NiTiNb SMA wires were activated by applying direct heat or electrical current, thereby providing a prestressing force. Finally, an FRP overlay was subsequently bonded to the repaired member to bridge the crack. This new approach was adopted by Zheng et al. (Zheng and Dawood, 2017; Zheng et al., 2018) and used for fatigue strengthening of edge-cracked steel plates. The results showed that the fatigue life of the steel plate that adopted this new approach was over 26 times longer than that of the unpatched steel plates.

In order to further evaluate the effectiveness of the SMA-CFRP composite in steel structures, the SMA-CFRP composites were used for the flexural strengthening of cracked steel beams in this study. The recovery force of NiTiNb-SMA wires with different prestrain levels and the bonding behavior of NiTiNb-SMA wires to the CFRP sheet was first studied to determine the fabrication of SMA patches. Then, SMA patches were combined with CFRP sheets for notched steel beam flexural strengthening. The strengthening effect of three reinforcement methods was compared through the four-point loading. The formula for the maximum allowable moment of the strengthened beams with SMA-CFRP composites was also derived.

Experimental methods

Material properties

The strengthened steel beams contain five materials: steel, CFRP, NiTiNb-SMA, CFSR-A/B adhesive for CFRP sheet impregnation, and Lica-131 adhesive for bonding the impregnated CFRP sheets. The two types of adhesive were used for the preparation of CFRP tabs, SMA/CFRP composites, and strengthened steel beams. The contents of Ni, Ti, and Nb in SMA wires were 48.6%, 36.6%, and 14.7%, respectively, based on manufactural data. The stress-strain curves and images of coupons for all materials are presented in Figure 1, and the main mechanical properties are listed in Table 1.

Optimal prestrain of SMA wire

According to a recent study (Hosseini et al., 2018), the recovery force is different for annealed SMA wire with varied prestrain. To obtain the maximum recovery force of SMA wire, the recovery force with different prestrain was tested. SMA can maintain the deformation and display shape memory effect when fully transforming from austenite to martensite under load. As shown in Figure 1(d), the completion point of the martensite transformation of SMA wire is approximately a prestrain of 12%; thus, the following six grades of prestrain were selected: 12%, 14%,

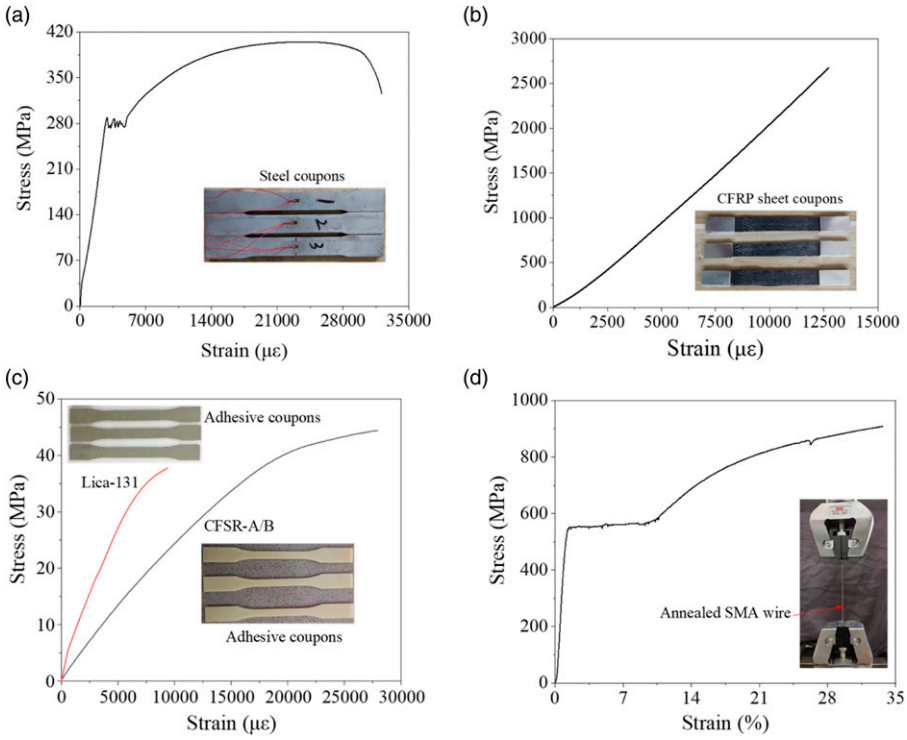

Figure 1. Stress–strain curves of (a) steel, (b) CFRP, (c) adhesive, and (d) SMA.

Table 1. Matrix of mechanical properties of materials.

Materials	Elastic modulus (GPa)	Yield strength (MPa)	Ultimate strength (MPa)
Steel	214.2	264.6	404.8
CFRP sheet	199.2	–	2398.8
CFSR-A/B adhesive	2.1	–	43.8
Lica-131 adhesive	5.7	–	39.2
SMA wire (annealed)	49.9	–	908.2

16%, 18%, 20%, and 22%. Three specimens were tested for each prestrain, and the recovery force is shown in Figure 2. It is clear that the maximum recovery force of 274 MPa is found for specimens with a prestrain of 12%. Thereafter, SMA wire with a prestrain of 12% was used for notched steel beam strengthening.

SMA-CFRP bonding performance

Sufficient bonding between the SMA wire and CFRP sheet is important for the prestressing retention of SMA wire and the workability of the strengthened system. Inspired by the previous study (Zheng et al., 2018), the embedded length (30 mm, 60 mm, and 120 mm) of the single SMA wire and the spacing between neighbouring wires (three wires in total with an embedment length of 120 mm) are considered to study the SMA wire bond capacity in a CFRP patch via pull-out tests. The test specimen was fabricated by

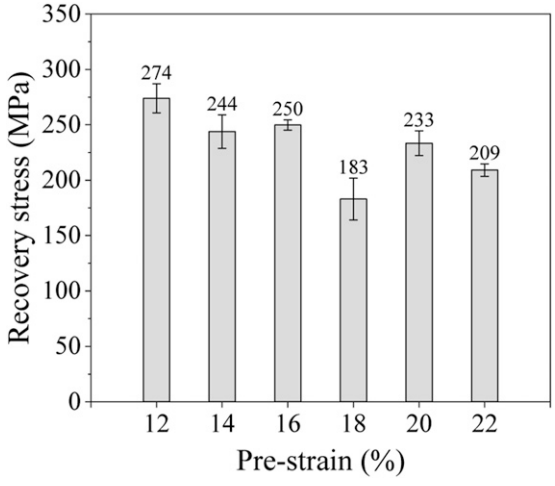

Figure 2. Recovery force of SMA wire with different prestrain grades.

sandwiching the SMA wire between two layers of the CFRP sheet, as shown in Figure 3(a). The CFRP sheet was impregnated with CSFR-A/B adhesive and then cured at room temperature for at least 24 h. The ultimate stress of the SMA wire is presented in Figure 3(b), which increases with the embedment length. Because the recovery stress of the SMA is 274 MPa, an embedment length of 120 mm was selected to ensure a sufficient margin of safety for the SMA patch. Figure 3(c) shows that the spacing of SMA wires has little effect on the ultimate stress. Considering the convenience of fabrication, a wire spacing of 1 mm was selected.

Notched steel beam strengthened by SMA-CFRP composites

Specimen design. Three strengthening methods were considered to investigate the strengthening effect of SMA-CFRP composite on the notched steel beam, as presented in Table 2. For the specimen identification, B, C, and S represent the notched steel beam, CFRP sheet strengthening, and SMA patch strengthening, respectively.

Hot rolled steel beams with a grade of Q235 were used in this study. Due to testing setup limitations and to be consistent with our previous work, the same dimension of steel beam was used (Li et al., 2019). As presented in Figure 4, the steel beam has a length of 1200 mm, a height of 120 mm, a flange width of 74 mm, and a web thickness of 5 mm. The clear span of the strengthened steel beam was 1100 mm, and the loading points were 200 mm apart. Eight steel stiffeners were welded to each beam at two loading points on either side of the web to prevent premature flange buckling and web crushing. A gap for the stiffeners at the loading points was designed to not interfere with SMA patch bonding to the top of the tension flange. To simulate the fatigue damage, a notch with a length of 14.4 mm was machined into the tension flange and web.

Preparation of specimens. Figure 5 illustrates the preparation of the steel beam strengthened with SMA-CFRP composites. Step 1 shows the SMA patch fabrication. SMA wires with a prestrain of 12% were arranged at a spacing of 1 mm, and both ends of the SMA wires were sandwiched by four impregnated CFRP sheets using Lica-131 adhesive. Two types of SMA patches were manufactured, and the only difference is the width of the patch. The SMA patch with a width of 74 mm contains 35 SMA wires, while the SMA patch with a width of 34 mm contains 15 SMA wires. These two types of patches were bonded to the bottom and top of the tension flange. Step 2 shows the strengthening area marking. The CFRP sheet bonding area was marked to

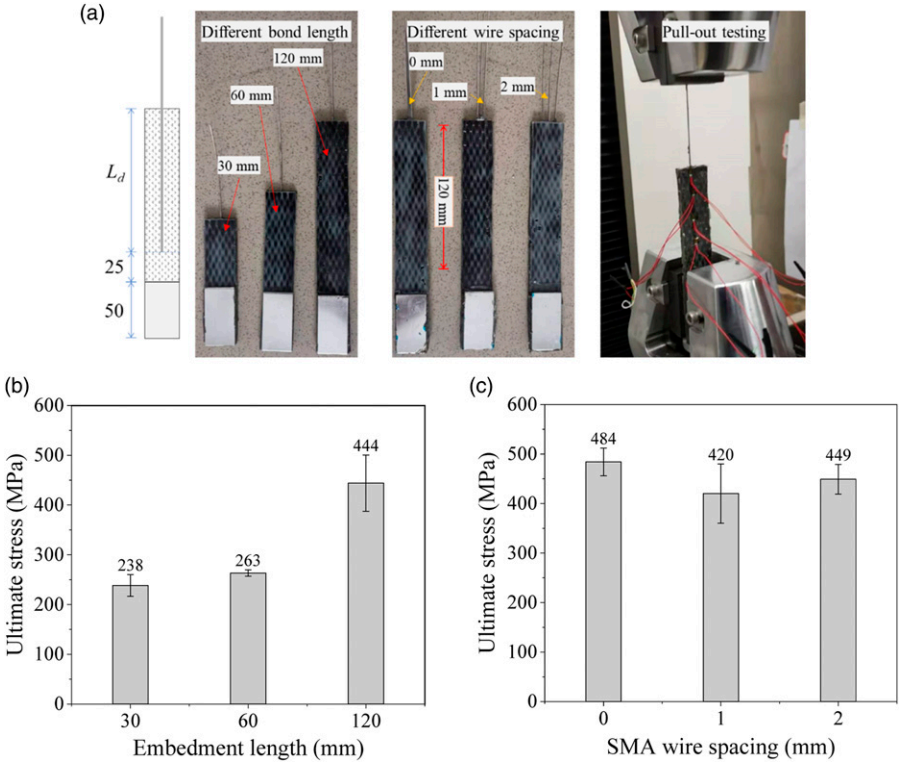

Figure 3. SMA-CFRP bonding test: (a) specimen and test setup, (b) ultimate stress of individual SMA wires with different embedment lengths, and (c) ultimate stress of individual SMA wires with different spacings.

Table 2. Design of specimens and test results.

Specimen	With/without notch	Strengthening method	Yield load (kN)	Yield deflection (mm)	Ultimate load (kN)	Flexural stiffness (kN/mm)
B0	Without	–	52.8	2.88	93.4	18.3
B1	With	–	15.9	1.31	39.0	12.1
BC	With	CFRP sheet	26.8	1.67	54.4	16.1
BS1	With	SMA patch	26.5	1.74	53.3	15.2
BS2	With	SMA patch	26.9	1.61	52.4	16.7
BS3	With	SMA patch	27.4	1.72	55.6	15.9
BSC1	With	SMA-CFRP composite	37.2	1.91	73.2	19.5
BSC2	With	SMA-CFRP composite	37.9	2.02	70.9	18.8
BSC3	With	SMA-CFRP composite	35.1	1.86	65.6	18.8

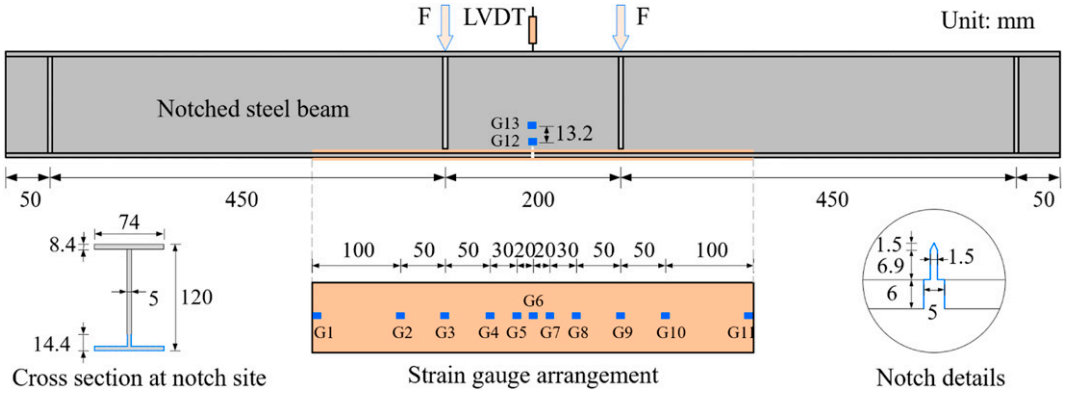

Figure 4. Geometry of the strengthened steel beam and arrangement of the strain gauges.

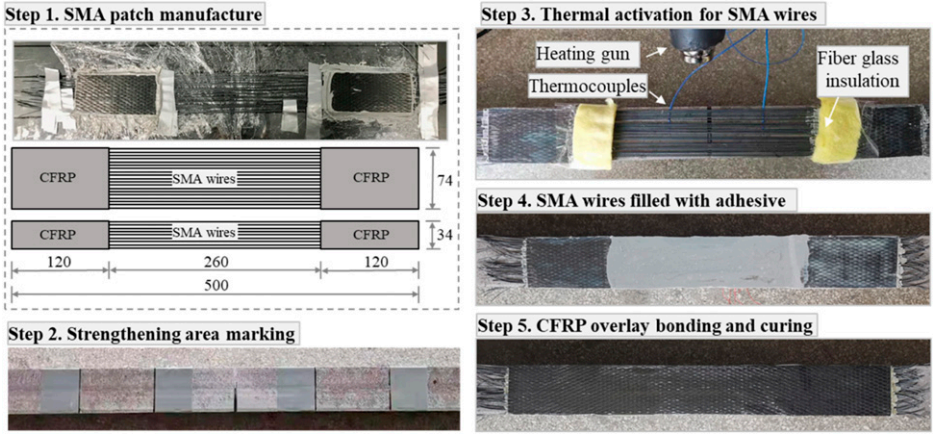

Figure 5. Preparation of notched steel beams strengthened with SMA-CFRP composite.

ensure that the notch was located in the middle of the SMA patch. The Lica-131 adhesive was used to bond the SMA patch to the steel tension flange and cured at room temperature for 7 days. Step 3 shows the thermal activation for SMA wires. A heating gun was used for the SMA wires' thermal activation, and fiberglass insulation was applied to block high temperatures and avoid debonding of SMA patches from the steel beam. Thermocouples were used to

monitor the temperature change. Step 4 shows the SMA wires filled with adhesive. Lica-131 was used to fill the SMA wires area after the wires were cooled to room temperature. The thickness of the filled adhesive was ensured to be equal to the SMA patch, and the surface of the filled adhesive was smoothed by a PVC plate so that the CFRP overlay could be evenly bonded to this surface. Step 5 shows the CFRP overlay bonded to the surface by CFSR-A/B adhesive. After this step, the steel beam with SMA-CFRP composites is complete. Based on the recovery stress (274 MPa) of a SMA wire, the SMA/CFRP composite would yield a prestress of 13.98 kN.

The preparation process for the steel beam strengthened with SMA patches includes steps 1–3, as described above. For the steel beam strengthened with a CFRP sheet, a CFRP sheet with a length of 500 mm and a width of 74 mm was impregnated with CFSR-A/B adhesive first and sufficiently cured; then, the cured CFRP sheet was bonded to the tension flange of the notched steel beam using Lica-131 adhesive. The manufactured specimens are presented in Figure 6.

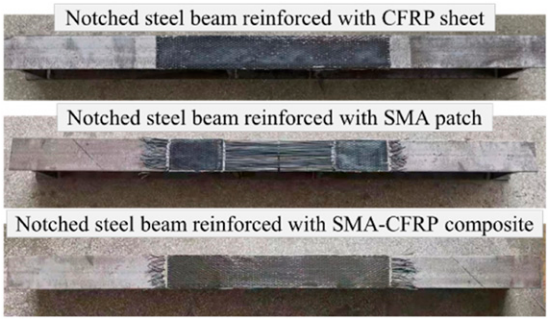

Figure 6. Manufactured specimens.

Loading protocol and data acquisition. Four-point bending tests were conducted in a servo-hydraulic SDS500 testing machine with a maximum capacity of 500 kN, as shown in Figure 7. Specimens were tested under static load by displacement control at a rate of 3 mm/min. Loading was continued until the specimens could not bear the loads. The strain distribution at the bottom of the CFRP sheet was measured using 11 2 mm long strain gauges, which were mounted along the longitudinal centreline of the CFRP sheet, as presented in Figure 4. A strain gauge (G12) was mounted at the notch tip. Mid-span deflection was measured using a linear variable differential transformer (LVDT), as shown in Figure 7. All data were automatically recorded by a data logger (DH3820).

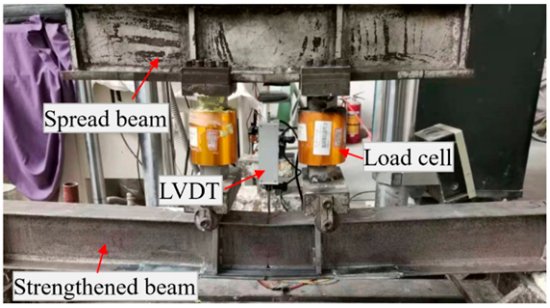

Figure 7. Four-point bending test setup.

Results and discussion

Load-deflection curves

As illustrated in Figure 8, different failure modes are observed for each type of specimen. The CFRP sheet was debonded and cracked at mid-span for the specimen BC. The SMA wires became entangled in the specimen BS due to notch expansion, but the SMA patch remained connected to the steel beam. Although the CFRP overlay was debonded and fractured in specimens BSC1 and BSC3, the SMA patch remained bonded to the steel beam, demonstrating that the SMA-CFRP composite has potential use in steel structure rehabilitation.

The mid-span deflection curves are compared in Figure 9. Compared with specimens B0 and B1, it can be seen that the notch significantly degraded the flexural performance. Before the load reached 52.82 kN, specimen B0 showed a linear load-deflection relationship. After that, the steel beam flange yielded, and the deflection showed an accelerated increasing trend with increasing load. When the load reached the maximum of 93.49 kN, the deflection decreased as the load increased. For specimen B1, before the load reached 15.90 kN, the deflection increased linearly with increasing load. After that, the notch tip yielded, and the deflection increased rapidly as the load increased until the maximum load of 36.98 kN. Then, the beam failed as the web notch greatly expanded.

A much higher load capacity and a prolonged elastic stage were found for specimen BC. A linear load-deflection relationship was observed until the load reached 26.8 kN. Then, the increase in deflection accelerated with increasing load, indicating that the notch tip was yielded. The CFRP sheet started to crack when the load reached 51.38 kN and completely fractured when the load reached 54.35 kN. After that, the load suddenly decreased, and the load-deflection curve followed that of specimen B1, as only the steel beam bears the load. A failure mode with CFRP debonding and fracture for specimen BC is shown in Figure 9.

A similar load-deflection trend was found for specimen BS at the elastic stage. When the load reached 26.51 kN, the notch tip yielded, and the deflection accelerated. When the load increased to 53.35 kN, the deflection steadily

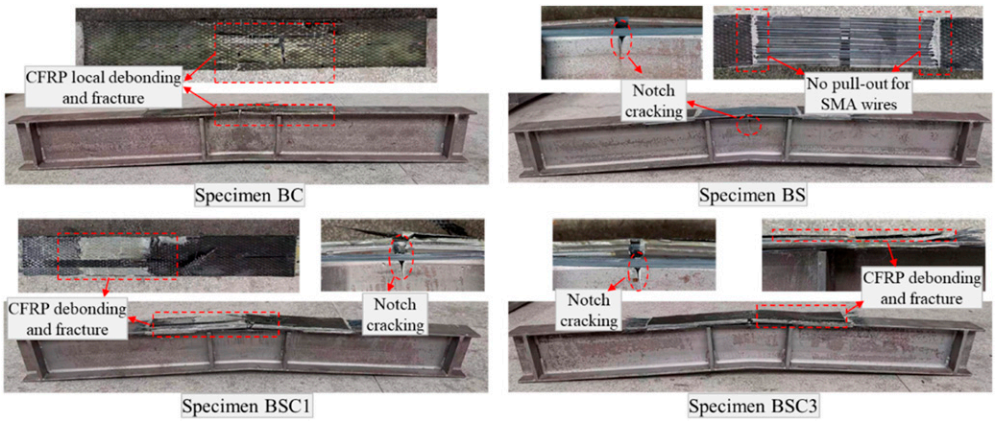

Figure 8. Failure modes of the specimens.

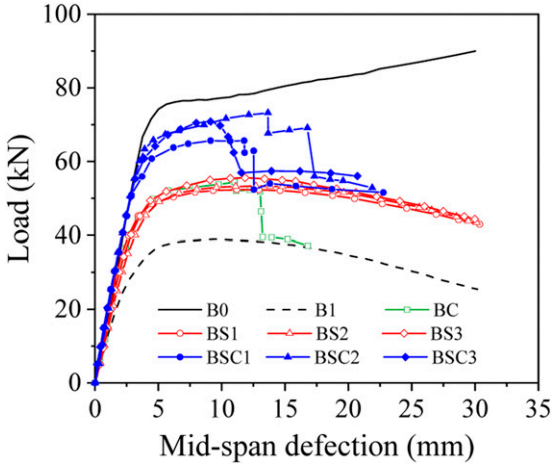

Figure 9. Load-deflection curves.

decreased as the load increased. Compared to specimen BC, there was no sudden load drop for the load-slip curve. This phenomenon indicates that SMA patch strengthening increases the load capacity and enhances ductility for notched steel beams. The failure mode of specimen BS is shown in Figure 9. As shown, the notch was significantly opened, but no pull-out phenomenon was observed for SMA wires from the SMA patch, indicating the applicability of the SMA patch.

For specimen BCS, it is clear that the elastic stage is much longer after strengthening by the SMA-CFRP composite and close to the load response of specimen B0 (intact beam). After reaching the yield loads (35.05 kN for BCS1, 37.15 kN for BCS2, and 37.96 kN for BCS3), the CFRP sheet began to crack for specimens BCS1 and BCS2, while CFRP sheet debonding was observed for specimen BCS3. This is the reason for the load-deflection curve change of the load-drop phenomenon. After the CFRP sheet fractured and debonded, the load-deflection curve followed specimen BS.

Load-carrying capacity and flexural stiffness

In this study, the maximum value of the load in the initial linear section of the load deflection curve was defined as the yield load, and the maximum load of the load-deflection curve was defined as the ultimate load. The yield loads, ultimate loads, and corresponding deflections are given in Table 2. The yield loads and ultimate loads are also presented in Figure 10. Compared with specimen B1, the yield loads of specimens BC, BS, and BCS are increased by 68.6%, 66.7%, and 130.8%, respectively. The ultimate loads of specimens BC, BS, and BCS are increased by 39.5%, 36.7%, and 79.2%, respectively. This indicates that the CFRP sheet and SMA patch have a similar strengthening effect, while the SMA-CFRP composite has a much higher strengthening effect. Compared to specimen B0, specimen BCSs (strengthened by SMA-CFRP composites) restored the load-carrying capacity of the notched steel beam to 74.8% of that of the intact beam.

The slope of the load-deflection curve at the elastic stage of the test beam was defined as the flexural stiffness and is presented in Figure 11. Similar to the increase in load capacity, the flexural stiffness was increased by different strengthening methods. The strengthening methods of the CFRP sheet and SMA patch have comparable effects on flexural stiffness. Compared with specimen B1 (notched steel beam), the flexural stiffness of specimens BC and BS increased by 33.1% and 32.2%, respectively. The SMA patch shows a slight strengthening effect on flexural stiffness compared to the CFRP sheet because the elastic modulus of SMA is less than that of the CFRP sheet. In contrast, the SMA-CFRP composite demonstrated approximately twice the strengthening effect on the flexural stiffness as the individual material of CFRP or SMA, which brings an increase of 57.9% in the flexural stiffness.

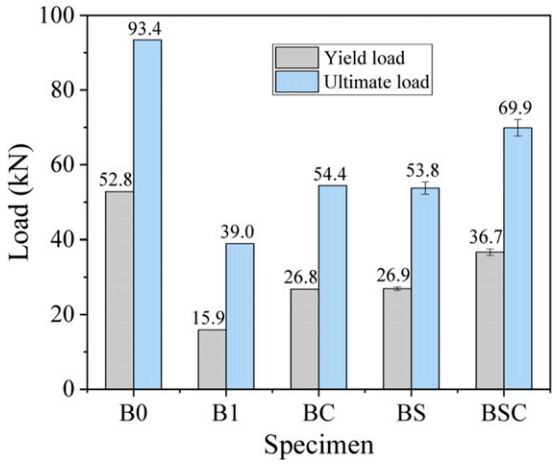

Figure 10. Load capacity of the specimens.

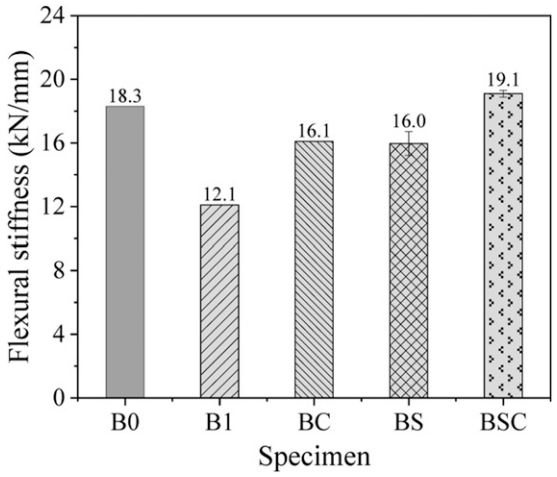

Figure 11. Flexural stiffness of the specimens.

Compared with specimen B0 (intact steel beam), the flexural stiffnesses of specimens BC, BS, and BCS are restored to 87.51%, 87.02%, and 103.76% of the intact steel beam, respectively. This indicates that the three strengthening methods can significantly improve the flexural stiffness of the notched steel beam. The improvement due to SMA and CFRP is equivalent, and the combined reinforcement effect of the SMA-CFRP composite is the best and even exceeds the stiffness of intact beams.

Notch tip strain development

To compare the crack closure effect of different strengthening methods, the notch tip strain development with the load increase is shown in Figure 12. All strains initially increase slowly with increasing load and begin to accelerate when the crack tip begins to yield. Comparing specimens BC and BS, it can be seen that both the CFRP sheet and SMA wires can slow down the strain growth rate at the crack tip, indicating that both strengthening methods can inhibit crack growth. Due to its relatively low stiffness compared to the CFRP sheet, the SMA patch strengthened steel beam showed a faster strain increase rate. Nevertheless, due to the recovery force of SMA wires after thermal activation, specimen BS showed a negative strain value at a low applied load and a greater notch-tip yield load than specimen BC. The notch tip yield load can be determined by the load when the strain begins to accelerate rapidly. This phenomenon is because the stiffness of SMA is smaller than that of CFRP; the thermally activated SMA generates prestress and produces a closure effect on the notch tip. Specimen BCS showed the best crack suppression effect. The strain growth rate at the notch tip was the slowest among all specimens, and the notch tip yield load was the largest, indicating that the composite reinforcement significantly reduced the notch tip stress and inhibited crack growth.

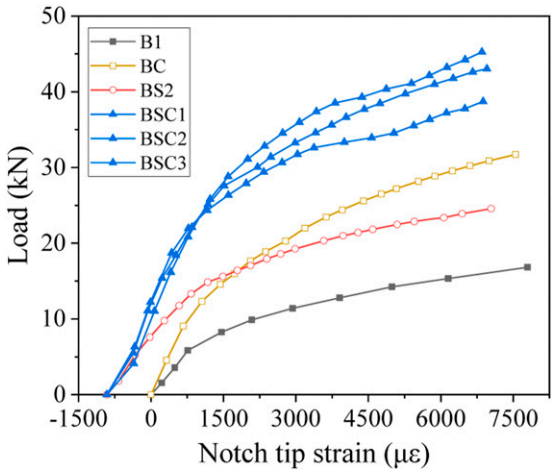

Figure 12. Notch tip strain increase with the load.

The notch tip yield loads are compared in Figure 13. It is clear that all strengthening methods increase the notch tip yield load. Compared with specimen B1, the notch tip yield load increased by 70% with CFRP strengthening (specimen BC), while it increased by 125% with SMA strengthening (specimen BS). This is because SMA can generate prestress at the notch tip after thermal excitation and largely reduce the stress concentration at the notch tip, while the hysteretic load-sharing of the CFRP sheet results in a weaker inhibition effect on the stress concentration at the notch tip. Compared to specimen B1, it can be found that the notch tip yield load of specimen BCS increased 230%, which is greater than the sum of the increased amplitudes of the strengthening methods of CFRP or SMA materials alone.

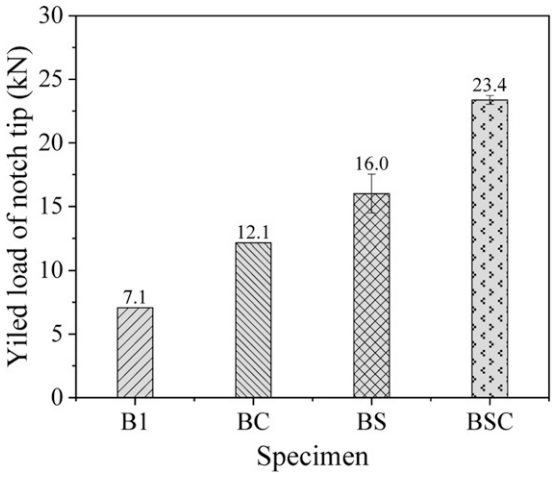

Figure 13. The load when the notch tip starts to yield.

From the above discussion, the SMA-CFRP composite strengthening greatly improves the load capacity, flexural stiffness, and ductility of notched steel beams. The mechanism of SMA-CFRP composite strengthening can be explained as follows: The presence of the SMA wires applies a compressive prestress force near the notch, thereby producing a closure effect on the notch tip. In addition, the combination of CFRP sheets adds additional stiffness, overcoming the low stiffness of SMA wires and reducing the magnitudes of the stresses caused by applied loads. Hence, SMA-CFRP composite strengthening can prevent the brittle failure of CFRP-reinforced steel beams due to CFRP fracture, exhibiting unique advantages over other single material strengthening methods.

CFRP strain distribution

For specimens strengthened with CFRP sheets and SMA-CFRP composites, the CFRP strain development at different locations was recorded by 11 strain gauges. The typical CFRP strain increase as the load increases is shown in Figure 14. Strain gauge G6, located at the mid-span, showed the fastest increase rate for all specimens because the CFRP sheet at the notch shares the most load. For specimen BC, no obvious strain increase was found at the other strain gauges (except G6) until it reached a load of 26.8 kN. After this load, the strain in G5 was significantly increased due to interfacial debonding from one side near the notch. When the load increased to 42 kN, interfacial debonding was observed at the other side of the notch, leading to accelerated strain growth for G7. When the load increased to 54.5 kN, the strain in G4 rapidly increased due to interfacial debonding propagating to the G4 location. Then, the CFRP sheet was fractured, and the strengthened steel beam failed. For specimen BSC1, strain development was similar to specimen BC. The strain in the other strain gauges developed following strain gauge G6 at the mid-span as the load increased. The closer to G6, the more rapid the strain can increase. Due to the bridging effect of SMA wires, the strain growth curves of G5 and G7 were relatively smooth. When the load increased to 56 kN, the strain in G4 suddenly increased, followed by G8 and G10. When specimen BSC1 failed, the strains in G4, G5, G7, G8, and G9 were almost equal, indicating that interfacial debonding appeared in the area from G4 to G9.

The longitudinal strain distribution in the CFRP sheet at different load levels is shown in Figure 15. When the loads were lower than the debonding loads, it was clear that strain was concentrated at the notch location (G6) in the middle of the beams. However, the strain concentration was reduced in the specimens strengthened with SMA-CFRP composite compared to specimen BC. This also indicates that SMA-CFRP strengthening is beneficial to the load capacity of the strengthened beams. After debonding loads, the maximum strain zone started to spread from the middle of the CFRP sheet to the sides. When the load increased to the ultimate loads, the strain curves in the pure bending section were almost horizontal, which implies that debonding propagated in this area. In addition, it was found that the horizontal strain distribution area of specimen BSC1 is larger than that of specimen BC at the ultimate loads, indicating that more CFRP sheets were fully utilized for specimen BSC1.

Theoretical analysis of a notched steel beam strengthened by SMA-CFRP composite

Basic assumption. The following assumptions were made in the analytical studies:

1. Steel is a uniform elastoplastic material, and the CFRP sheet is a linear elastic material.
2. The plane-section assumption for the steel beam after strengthening still holds.
3. SMA wires are perfectly embedded in two CFRP sheets so that no SMA wire slip occurs during bending.

Derivation of the notch tip yield moment and maximum allowable moment. It can follow the elastic-plastic method to design steel beams subjected to static or indirect dynamic loads. However, the depth of the plasticity area should be limited to a specific range, which is less than 0.125 times the cross height of the steel beam (Le et al., 2014). Based on this requirement, the notch tip yield moment and maximum allowable moment were derived. The maximum allowable moment is reached when the plastic area develops 0.125 times the section height of the steel beam at the notch tip (13.2 mm in this study). For the cracked steel beam

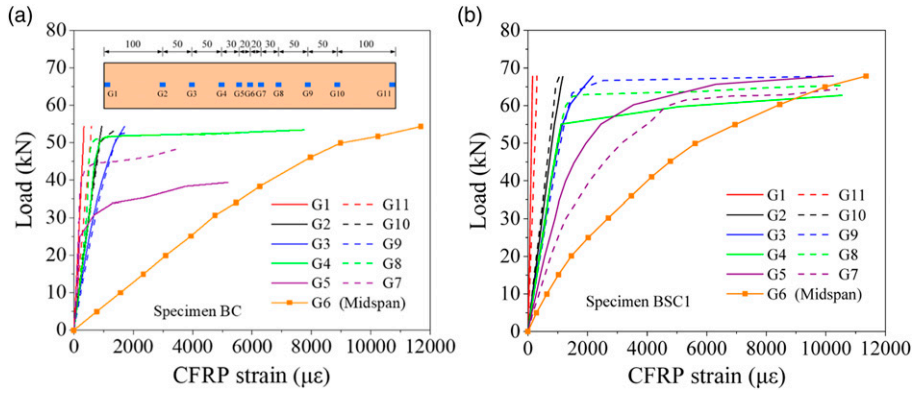

Figure 14. CFRP strain development as the load increased: (a) specimen BC and (b) specimen BSC1.

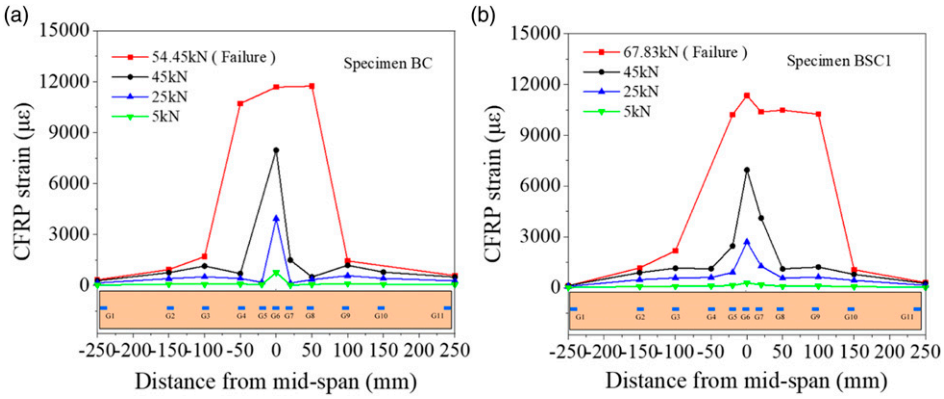

Figure 15. CFRP strain distribution at different loads: (a) specimen BC and (b) specimen BSC1.

strengthened with SMA-CFRP composites (the crack length is l located at the mid-span), the strain distribution along the notched section of the strengthened beams at the notch-tip yield state and the maximum load-bearing state is presented in Figure 16.

When the notch tip starts to yield (see Figure 16(a)), equation (1) can be given based on the force equilibrium,

$$\begin{aligned} &1/2\left(\varepsilon_{1y}+\frac{h_1-x_y-t}{h_1-x_y}\varepsilon_{1y}\right)bt+\frac{\left(h_1-x_y-t\right)^2}{2\left(h_1-x_y\right)}\varepsilon_{1y} \\ &d=1/2\varepsilon_{2y}x_yd+\alpha_0A_c\varepsilon_{cy}+\alpha_1\left(A_{s1}\varepsilon_{s1y}+A_{s2}\varepsilon_{s2y}\right) \end{aligned} \quad (1)$$

where x_y is the distance from the notch tip to the neutral axis, h_1 is the distance from the notch tip to the top of the beam, ε_{1y} is the compressive strain at the top of the beam, ε_{2y} is the notch tip strain, ε_{cy} is the CFRP strain, ε_{s1y} is the total strain of SMA wires at the top of the tension flange, ε_{s2y} is the total strain of SMA wires at the bottom of the tension flange, A_c is the section area of the CFRP sheet, A_{s1} is the section area of SMA wires at the top of the tension flange, A_{s2} is the section area of the SMA wires at the bottom of the tension flange, α_0 is the equivalent conversion factor of CFRP to steel, and α_1 is the equivalent conversion factor of SMA to steel.

According to equation (1), x_y can be calculated, and then the notch tip yield moment of the strengthened steel beams can be given as follows:

$$\begin{aligned} M_{y.steel}&=\frac{f_yI_{0.y}}{x_y} \\ M_{y.cfrp}&=E_{cfrp}A_c\varepsilon_{cy}e_{cy} \\ M_{y.sma}&=E_{sma}\left(30A_{s1}\varepsilon_{s1y}e_{sy}+35A_{s2}\varepsilon_{s2y}e_{cy}\right) \\ M_y&=M_{y.steel}+M_{y.cfrp}+M_{y.sma} \end{aligned} \quad (2)$$

where f_y is the steel yield stress corrected by the stress concentration factor; $I_{0.y}$ is the inertia moment of the combined section at the notch site; E_{cfrp} is the elastic modulus of the CFRP sheet; E_{sma} is the SMA elastic modulus (austenite); e_{sy} is the distance between the top of

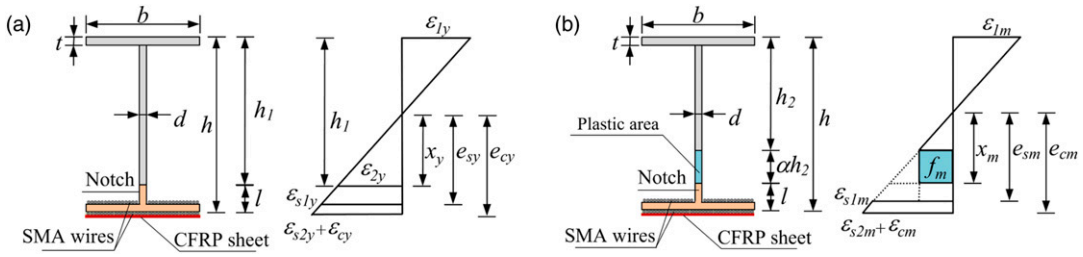

Figure 16. Strain distribution along the notched section of the steel beam strengthened with SMA-CFRP composite at the (a) notch tip yield state and (b) maximum allowable load-bearing state.

Table 3. Comparison of the analytical and experimental results.

Specimen	Mean yield moment (kN·m)		Deviation, %	Mean ultimate moment (kN·m)		Deviation, %
	$M_{y.exp.}$	$M_{y.ana.}$		$M_{m.exp.}$	$M_{m.ana.}$	
BC	2.73	2.71	0.73	5.32	4.87	8.5
BS	3.60	3.38	6.10	5.85	6.34	8.4
BSC	5.25	4.71	10.3	7.58	7.04	7.1

the tension flange and the neutral axis; and e_{cy} is the distance between the bottom of the tension flange and the neutral axis.

When the strengthened steel beam reaches the maximum allowable load-bearing state (the plastic area at the web develops 0.125 times the section height of the steel beam), the strain distribution is presented in Figure 16(b). Stress concentration effects are not considered due to plastic deformation in this state. Thus, equation (3) can be given based on the force balance of the section,

$$\begin{aligned} &1/2\left(\varepsilon_{1m}+\frac{h_2-x_m-t}{h_2-x_m}\varepsilon_{1m}\right)btE_{steel} \\ &+1/2\frac{(h_2-x_m-t)^2}{h_1-x_m}\varepsilon_{1m}dE_{steel}=ah_2df_m \\ &+1/2(x_m-ah_2)df_m+A_c\varepsilon_{cm}E_{cfrp} \\ &+(A_{s1}\varepsilon_{s1m}+A_{s2}\varepsilon_{s2m})E_{sma} \end{aligned} \tag{3}$$

where x_m is the distance from the notch tip to the neutral axis; h_2 is the distance from the top of the plastic area to the top of the beam; α is the plastic development coefficient, which is 0.125 in this study; ε_{1m} is the compressive strain at the top of the beam; f_m is the steel yield stress; ε_{cm} is the CFRP strain; ε_{s1m} is the total strain of SMA wires at the top of the tension flange; ε_{s2m} is the total strain of SMA wires at the bottom of the tension flange; and E_{steel} is the steel elastic modulus.

According to equation (3), x_m can be calculated; then, the maximum allowable moment of the strengthened steel beams can be given as follows:

$$\begin{aligned} M_{m.steel}&=\frac{f_mI_{0.m}}{x_m} \\ M_{m.cfrp}&=E_{cfrp}A_c\varepsilon_{cm}e_{cm} \\ M_{m.sma}&=E_{sma}(30A_{s1}\varepsilon_{s1m}e_{sm}+35A_{s2}\varepsilon_{s2m}e_{cm}) \\ M_m&=M_{m.steel}+M_{m.cfrp}+M_{m.sma} \end{aligned} \tag{4}$$

where $I_{0.m}$ is the inertia moment of the combined section considering the plastic development depth; e_{sm} is the distance from the top of the tension flange to the neutral axis; and e_{cm} is the distance from the bottom of the tension flange to the neutral axis.

Validation of the proposed analytical model. According to equations (2) and (4), the mean notch tip yield moment and mean maximum allowable moment of the notched steel beam strengthened with SMA-CFRP composite are calculated and listed in Table 3. Also the results of specimen BC and BS are presented in the table. The average experimental notch tip yield moments of the BSC beams were 5.25 kN·m, respectively. The analytical notch tip yield moment was 4.71 kN·m. The average deviation between the analytical and experimental results is less than 10.3%. The experimental maximum moments (when the plastic depth developed 13.2 mm from the notch tip, determined by the yield strain recorded in G13) of the BSC beams were 7.58 kN·m, respectively. The analytical maximum moment was 7.04 kN·m. The deviation between the analytical and experimental results is less than 7.1%.

The deviation of three types of specimens were in acceptable range, proving the accuracy of the proposed analytical equations.

Conclusions

In this study, the effectiveness of the SMA-CFRP composites on the flexural strengthening of notched steel beams was evaluated in notch tip yield load, ultimate load, and flexural stiffness. Then the load capacity of notched steel beams strengthened by SMA-CFRP composite was derived. The following conclusions can be drawn:

1. The recovery stress of NiTiNb-SMA and the bond capacity of SMA and CFRP sheet were investigated. After thermal activation, a recovery stress of 273.86 MPa can be generated for a single SMA wire. The bond strength of SMA and CFRP increased with the increase in embedded length but only slightly changed with the SMA wire spacing increase. An embedded length of 120 mm can prevent SMA debonding failure caused by recovery stress and can be adopted for SMA-CFRP patch preparation.
2. SMA-CFRP composite strengthening can improve the load capacity and stiffness of notched steel beams. Compared to notched steel beams, the ultimate loads of the CFRP sheet, SMA patch, and SMA-CFRP composite reinforced beams are increased by 39.5%, 36.7%, and 79.2%, respectively; the stiffness of CFRP, SMA, and SMA-CFRP composite reinforced beams increased by 33.1%, 32.2%, and 57.9%, respectively.
3. SMA-CFRP composite strengthening can significantly inhibit crack propagation as well. The notch yield load for steel beam reinforced with CFRP sheet, SMA patch, and SMA-CFRP composite were increased 70%, 125%, and 230%, respectively. In addition, the failure modes of SMA-CFRP composite strengthened beams were CFRP sheet debonding or fracture, and the SMA-CFRP patch still bonded on the steel beams, indicating the effectiveness of the proposed SMA-CFRP strengthening method.
4. Analytical formulas were proposed to calculate the notch tip yield moment and maximum allowable moment for SMA-CFRP composite strengthened steel beams. The average deviation of the notch tip yield moment and maximum allowable moment between the analytical and experimental results are less than 10.3% and 7.1%, respectively, proving the accuracy of the proposed analytical equations.

Declaration of conflicting interests

The author(s) declared no potential conflicts of interest with respect to the research, authorship, and/or publication of this article.

Funding

The author(s) disclosed receipt of the following financial support for the research, authorship, and/or publication of this article: This work was supported by a grant from the National Natural Science Foundation of China (Project No. 52178278, 51778151, 52208309); The Department of Education of Guangdong Province, China (Project No. 2021KCXTD030); The Innovation Research for Postgraduates of Guangzhou University (No. 2022GDJC-D18).

ORCID iD

Junhui Li https://orcid.org/0000-0001-5887-530X

References

Abdy AI, Hashemi MJ and Al-Mahaidi R (2018) Fatigue life improvement of steel structures using self-prestressing CFRP/SMA hybrid composite patches. *Engineering Structures* 174: 358–372.

Bollas D, Pappas P, Parthenios J, et al. (2007) Stress generation by shape memory alloy wires embedded in polymer composites. *Acta Materialia* 55(16): 5489–5499.

Cladera A, Weber B, Leinenbach C, et al. (2014) Iron-based shape memory alloys for civil engineering structures: an overview. *Construction and Building Materials* 63: 281–293.

Deng J, Fei Z, Li J, et al. (2023) Fatigue behaviour of notched steel beams strengthened by a self-prestressing SMA/CFRP composite. *Engineering Structures* 274: 115077.

Deng J and Lee MMK (2007) Behaviour under static loading of metallic beams reinforced with a bonded CFRP plate. *Composite Structures* 78(2): 232–242.

Deng J, Lee MMK and Moy SSJ (2004) Stress analysis of steel beams reinforced with a bonded CFRP plate. *Composite Structures* 65(2): 205–215.

Deng J, Li J and Zhu M (2022) Fatigue behavior of notched steel beams strengthened by a prestressed CFRP plate subjected to wetting/drying cycles. *Composites Part B: Engineering* 230: 109491.

El-Tahan M, Dawood M and Song G (2015) Development of a self-stressing NiTiNb shape memory alloy (SMA)/fiber reinforced polymer (FRP) patch. *Smart Materials and Structures* 24(6): 065035.

El-Tahan M and Dawood M (2018) Bond behavior of NiTiNb SMA wires embedded in CFRP composites. *Polymer Composites* 39(10): 3780–3791.

Fritsch E, Izadi M and Ghafoori E (2019) Development of nail-anchor strengthening system with iron-based shape memory alloy (Fe-SMA) strips. *Construction and Building Materials* 229: 117042.

Galvez P, Abenojar J and Martinez MA (2019) Effect of moisture and temperature on the thermal and mechanical properties of a ductile epoxy adhesive for use in steel structures reinforced with CFRP. *Composites Part B: Engineering* 176: 107194.

Ghafoori E, Hosseini A, Al-Mahaidi R, et al. (2018) Prestressed CFRP-strengthening and long-term wireless monitoring of an old roadway metallic bridge. *Engineering Structures* 176: 585–605.

Ghafoori E, Schumacher A and Motavalli M (2012) Fatigue behavior of notched steel beams reinforced with bonded CFRP plates: determination of prestressing level for crack arrest. *Engineering Structures* 45: 270–283.

Gholampour A and Ozbakkaloglu T (2018) Understanding the compressive behavior of shape memory alloy (SMA)-confined normal- and high-strength concrete. *Composite Structures* 202: 943–953.

He J, Xian G and Zhang YX (2020) Effect of moderately elevated temperatures on bond behaviour of CFRP-to-steel bonded joints using different adhesives. *Construction and Building Materials* 241: 118057.

Hollaway LC (2010) A review of the present and future utilisation of FRP composites in the civil infrastructure with reference to their important in-service properties. *Construction and Building Materials* 24(12): 2419–2445.

Hosseini A, Ghafoori E, Motavalli M, et al. (2019) Development of prestressed unbonded and bonded CFRP strengthening solutions for tensile metallic members. *Engineering Structures* 181: 550–561.

Hosseini E, Ghafoori E, Leinenbach C, et al. (2018) Stress recovery and cyclic behaviour of an Fe–Mn–Si shape memory alloy after multiple thermal activation. *Smart Materials and Structures* 27(2): 025009.

Hu L and Feng P (2021) Prestressed CFRP-reinforced steel columns under axial and eccentric compression. *Composite Structures* 268: 113940.

Hu L, Feng P, Gao W, et al. (2022) Flexural behavior of light steel purlins reinforced by prestressed CFRP laminates. *Thin-Walled Structures* 174: 109125.

Izadi M, Hosseini A, Michels J, et al. (2019) Thermally activated iron-based shape memory alloy for strengthening metallic girders. *Thin-Walled Structures* 141: 389–401.

Izadi MR, Ghafoori E, Motavalli M, et al. (2018a) Iron-based shape memory alloy for the fatigue strengthening of cracked steel plates: effects of re-activations and loading frequencies. *Engineering Structures* 176: 953–967.

Izadi MR, Ghafoori E, Shahverdi M, et al. (2018b) Development of an iron-based shape memory alloy (Fe-SMA) strengthening system for steel plates. *Engineering Structures* 174: 433–446.

Ke L, Li C, He J, et al. (2020) Effects of elevated temperatures on mechanical behavior of epoxy adhesives and CFRP-steel hybrid joints. *Composite Structures* 235: 111789.

Kianmofrad F, Ghafoori E, Elyasi MM, et al. (2017) Strengthening of metallic beams with different types of pre-stressed un-bonded retrofit systems. *Composite Structures* 159: 81–95.

Le Z, Zhang J and Bai Y (2014) Experimental study and theoretical analysis of flexural beam strengthened by CFRP. *Journal of Shenyang University(Natural Science)* 26(5): 391–395.

Li H, Liu Z-q and Ou J-p (2008) Experimental study of a simple reinforced concrete beam temporarily strengthened by SMA wires followed by permanent strengthening with CFRP plates. *Engineering Structures* 30(3): 716–723.

Li J, Deng J, Wang Y, et al. (2019) Experimental study of notched steel beams strengthened with a CFRP plate subjected to overloading fatigue and wetting/drying cycles. *Composite Structures* 209: 634–643.

Li J, Wang Y, Deng J, et al. (2018) Experimental study on the flexural behaviour of notched steel beams strengthened by prestressed CFRP plate with an end plate anchorage system. *Engineering Structures* 171: 29–39.

Li J, Zhu M and Deng J (2022) Flexural behaviour of notched steel beams strengthened with a prestressed CFRP plate subjected to fatigue damage and wetting/drying cycles. *Engineering Structures* 250: 113430.

Li L, Chen T, Gu X, et al. (2020) Heat activated SMA-CFRP composites for fatigue strengthening of cracked steel plates. *Journal of Composites for Construction* 24(6): 04020060.

Mohd Jani J, Leary M, Subic A, et al. (2014) A review of shape memory alloy research, applications and opportunities. *Materials and Design* 56: 1078–1113.

Parvin A and Raad J (2018) Internal and external reinforcement of concrete members by use of shape memory alloy and fiber reinforced polymers under cyclic loading-a review. *Polymers (Basel)* 10(4): 376.

Shahverdi M, Czaderski C and Motavalli M (2016) Iron-based shape memory alloys for prestressed near-surface mounted strengthening of reinforced concrete beams. *Construction and Building Materials* 112: 28–38.

Yu QQ and Wu YF (2017) Fatigue strengthening of cracked steel beams with different configurations and materials. *Journal of Composites for Construction* 21(2): 04016093.

Zareie S, Issa AS, Seethaler RJ, et al. (2020) Recent advances in the applications of shape memory alloys in civil infrastructures: a review. *Structures* 27: 1535–1550.

Zhao XL and Zhang L (2007) State-of-the-art review on FRP strengthened steel structures. *Engineering Structures* 29(8): 1808–1823.

Zheng B and Dawood M (2017) Fatigue strengthening of metallic structures with a thermally activated shape memory alloy fiber-reinforced polymer patch. *Journal of Composites for Construction* 21(4): 04016113.

Zheng BT, El-Tahan M and Dawood M (2018) Shape memory alloy-carbon fiber reinforced polymer system for strengthening fatigue-sensitive metallic structures. *Engineering Structures* 171: 190–201.